AIAA Propulsion and Energy Forum
August 24-28, 2020, VIRTUAL EVENT
AIAA Propulsion and Energy 2020 Forum

10.2514/6.2020-3557

Integrated Propulsive and Thermal Management System Design for Optimal Hybrid Electric Aircraft Performance

Philip Abolmoali*, Adam Donovan†, and Soumya S. Patnaik‡
Air Force Research Laboratory, Dayton, OH 45433

Patrick McCarthy§, Dominic Dierker¶, and Nick Jones#
PC Krause & Associates, Indianapolis, IN, 46268

Robert Buettner**
UES Inc., Dayton, OH, 45432

The use of hybrid-electric propulsion systems aboard aircraft present opportunities for improved vehicle range and endurance, reduced fuel burn, as well as lower acoustic and thermal signatures. The energy benefits anticipated by such architectures may be offset, however, by new thermal management challenges introduced by the heat generated within the components of a hybrid-electric power train. A system level modeling approach that integrates the propulsion and thermal management subsystems is therefore critical to providing insight into the various tradeoffs. The current paper explores the reduction in fuel consumption offered by a series hybrid propulsion system using an integrated system modeling approach. A numerical model of the propulsive, thermal management, and flight dynamics subsystems was developed to simulate component and system level performance of a fixed wing, 11901 lb. medium altitude long endurance (MALE) vehicle, conventionally driven by a turboprop engine. . A thermal management system was integrated with the propulsive subsystem which utilized closed loop fuel cooling for electrical devices within the hybrid drive train, as well as a Polyalphaolephin (PAO) coolant loop to absorb the heat from several aircraft level auxiliary heat loads. Ram air was utilized to provide a heat sink for the PAO cooling loop, as well as the fuel loop to ensure return-to-tank fuel temperature limits are maintained. For a notional 18 hour flight mission, with respect to the conventional propulsion system, a fuel savings of 750 lb. was obtained, despite a gain of 708 lb. associated with the added weight of electrical devices within the drive train.

I. Nomenclature

ACS	=	Air Cycle System
AFRL	=	Air Force Research Laboratory
DoF	=	Degree of Freedom

* Aerospace Engineer, Aerospace Systems Directorate, 1950 5th Street, Area B, Wright Patterson AFB 45433, AIAA Non-Member
† Associate Mechanical Engineer, Aerospace Systems Directorate, 1950 5th Street, Area B, Wright Patterson AFB 45433, AIAA Non-Member
‡ Senior Engineer, Aerospace Systems Directorate, 1950 5th Street, Area B, Wright Patterson AFB 45433, AIAA Senior Member.
§ Senior Lead Engineer, 4291 W 96th Street, Indianapolis, IN 46268, AIAA Non-Member
¶ Lead Engineer, 4291 W 96th Street, Indianapolis, IN 46268, AIAA Non-Member
# Lead Engineer, 4291 W 96th Street, Indianapolis, IN 46268, AIAA Non-Member
** Research Scientist, Aerospace Power & Propulsion Division, 4401 Dayton-Xenia Rd, Dayton OH 45432, AIAA Non-Member

Case #: 88ABW-2020-2507

FAR = Fuel – Air Ratio
GTOW = Gross Take-Off Weight
ICE = Internal Combustion Engine
ISA = International Standard Atmosphere
ISR = Intelligence, Reconnaissance, and Surveillance
PAO = Polyalphaolephin
PMSM = Permanent Magnet Synchronous Machine
PR = Pressure Ratio
TMS = Thermal Management System
VCS = Vapor Cycle System
WRSM = Wound Rotor Synchronous Machine

II. Introduction

Propulsive power for civil and military aircraft have historically been provided through the combustion of hydrocarbon fuels within reciprocating and gas turbine engines. In recent years, concerns over fossil fuel availability, noise radiation, and environmental emissions have led the aviation community to explore the integration of electric power sources to supplement the propulsive power produced by these conventional powerplants [1]. Hybrid electric propulsion architectures, in particular, seek to acquire the advantages offered by the relatively quiet, high efficiency operation of electrical devices, in addition to the energy-dense characteristics of fuel driven, internal combustion engines. Hybrid electric technology has already demonstrated success in the automotive industry, and researchers in industry, government, and academia are exploring its potential to reduce fuel consumption, improve aircraft range, and decrease acoustic and thermal signatures for aircraft. In the commercial sector, Bradley and Droney [2] summarize the results obtained regarding the impact of a hybrid electric power plant on the fuel consumption and noise on the SUGAR Volt (Subsonic Ultra Green Aircraft Research), which demonstrated emissions improvements as well as satisfying NASA goals for fuel burn. Hiserote [3] investigated the use of an ICE-driven, parallel hybrid propulsion system to quantify fuel consumption to conduct a 5 hour ISR mission for military applications and their results showed a 30.5% reduction in fuel consumption was realized in comparison to a traditional ICE driven aircraft. Steady progress has also been made in academic research to formulate novel methods for conceptual hybrid electric aircraft and energy subsystems design, notably at Georgia Tech [4], Aachen University of Technology [5], and Delft University of Technology [6].

Despite the promising results of the aforementioned studies, several reports within the literature suggest that the thermal management challenges associated with the adoption of an electrified drive train may offset the benefits that are offered by hybrid propulsion systems [9,10]. Significant heat loads may still arise, despite the relatively high conversion efficiencies of electric devices [8]. Ultimately, the added weight, driving power, and drag penalties incurred by a TMS to reject the heat generated by a hybrid electric system will adversely affect vehicle level performance. Rheume and Lents [9] investigated the use of a 5 MW parallel hybrid architecture on a single aisle commercial aircraft to study the impact of the TMS on fuel consumption. Separate cooling circuits of oil and a 50% propylene glycol/water coolant were used to absorb heat from engine related loads, in addition to battery and motor drive heat loads, respectively. Fuel and fan duct bypass air were utilized as heat sinks for the engine heat loads, while ram air was utilized as a sink for the coolant. Results determined that a 3.4% increase in fuel consumption was observed during takeoff, climb, and cruise. Kim et al. [10] utilized an integrated design approach to study the impact of a TMS design on vehicle fuel consumption for a 150 passenger, turboelectric blended wing body aircraft flying a 3000 nautical mile mission. Traditional TMS architectures were proposed to reject the heat loads, including a fuel thermal management system, a vapor cycle system, and a combination of the two. Even utilizing state-of-the-art technology, a suitable turboelectric architecture was not found to be feasible.

For conventionally-driven commercial and military aircraft, thermal management is a persistent design challenge driven by growing power demands for advanced mission capability, and the migration towards electrified substitutes for traditional aircraft energy subsystems [11]. Walters et al [11] note that present thermal management concerns are indicative of a failure to properly integrate the thermal management system design into the aircraft system of systems design. Therefore, the modern approach to address thermal management concerns and achieve superior vehicle level performance has been to perform integrated vehicle subsystem designs, which may perform sub-optimally at the subsystem level. Given the novelty of hybrid-electric propulsion systems for aircraft, and their potential for significant interactions with the aircraft TMS, it is expected that an integrated systems design and analysis must be performed to account for any undesirable behavior that may appear during flight operations, in addition to bounding the achievable benefits offered by such propulsion concepts.

III. Proposed Study

To more thoroughly assess the benefits of hybrid electric propulsion in the presence of significant thermal management requirements, system modeling approach that integrates the propulsive and thermal management subsystems was undertaken. A MATLAB/Simulink based model was developed and a comparative numerical study was performed to quantify the difference in fuel consumption achieved when utilizing a hybrid propulsive architecture. A fixed wing medium altitude long endurance (MALE) aircraft of 11901 lb. gross takeoff weight (GTOW) flying a notional 18 hour mission was chosen as the representative case.. The air vehicle is conventionally powered by a turboprop engine, and was designed to possess similar performance to the engine in [19]. To simplify the analysis, no changes to the vehicle drag polar have been made when adopting a hybrid architecture. As an initial study, a series-hybrid configuration, as seen in Fig. 1, was investigated as a propulsive architecture for the air vehicle.

In the series-hybrid configuration, the prime mover may be a fuel driven reciprocating ICE (spark-ignition or Diesel) or a turbine engine. Mechanical power produced by the prime mover is transmitted to a generator producing electric power. A power conversion / control unit regulates the flow of electric power between platform loads, an energy storage system (i.e. battery), and a motor, which is utilized to drive a propeller for propulsive power. Notable advantages of the series hybrid configuration are the ability to operate the prime mover at an optimum torque and speed independent of driving conditions, and for distributed propulsion applications.

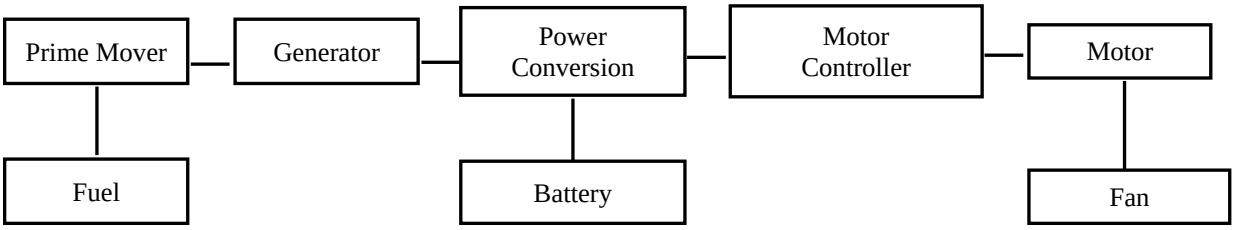

Fig. 1 Series-hybrid electric architecture

Integrated numerical models of propulsion, thermal management, and flight subsystems were developed using the ATTMOSphere toolset [12,14,15,16,17] and a 2.5DoF air vehicle model [13] to design and size the subsystems, as well as quantify the fuel consumption over the course of the mission. A simplified approximation to calculate fuel consumption is used by prescribing an empty weight of 4901 lb. to the conventionally powered aircraft, and attributing the remainder of the aircraft GTOW to fuel, a fraction of which will be burned over the course of the mission. By following this procedure, a comparison of the fuel consumption between the conventional and hybridized architectures may be approximated. The remainder of the paper presents numerical models of both the conventional and series hybrid propulsive architecture, their associated thermal management systems, as well as the design conditions and controls utilized to arrive at our results.

IV. System Design, Model Building and Analysis

A. Mission Profile

The altitude and flight Mach numbers for the mission under consideration are shown in Fig. 2. Mission segments were divided into the following sequence of unique operating conditions: climb – cruise – loiter. The reverse sequence were followed to return the vehicle to its initial conditions. Ground idle and take-off were explored under a different study.

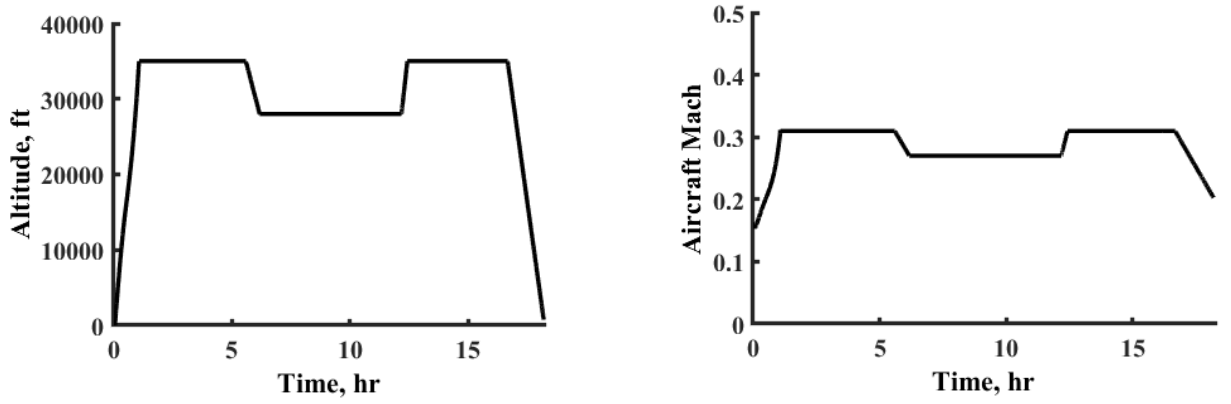

a) **b)**

Fig. 2 Notional aircraft mission: altitude and Mach variation

B. Air Vehicle Model

Engine models were coupled with a reduced order, 2.5DoF air vehicle model [13] in order to run integrated analysis to determine the effects of engine performance on the ability of the aircraft to operate under various mission profiles. While traditional 6DoF and 3DoF models have twelve and six integrators associated with their corresponding sets of six and three second-order differential equations of motion respectively, the 2.5DoF model has five integrators that correspond to two second-order force equations, and a first-order kinematic equation associated with coordinated turns. This coordinated turn expression couples the roll and yaw moments of the aircraft, and restricts movement to zero sideslip conditions. With this restriction, all turns can be expressed simply as a function of the aircraft's current bank angle and flight condition. The model uses drag polar aerodynamics based on CFD analysis to calculate the aircraft's drag, based on the lift corresponding to the aircraft's current angle of attack. The model controls $\dot{v}$, $\dot{\gamma}$, ψ and uses Nonlinear Dynamic Inversion (NDI) to command corresponding angle of attack, thrust, and bank angle commands. The corresponding thrust command is sent to the engine model, where the actual thrust and fuel flow values are calculated based on the current operating condition, and then sent back to the aero model. In instances where the thrust command cannot be met by the engine model, the controller adjusts the thrust commanded for the next time step until the engine model can generate enough thrust to get the aircraft back on its original desired path. The Simulink based 2.5DoF aircraft model is easily coupled with engine models to simulate and explore various flight metrics over the course of a given mission.

C. Propulsion and Thermal Management Subsystem Model Building

Engine and TMS sizing, design, and analysis was performed using the ATTMOSphere toolset [12,14,15,16,17] An express engine library developed as part of the AFRL Aircraft Power and Thermal Toolkit (APTT) provides a series of known engine designs for use in system level transient analysis of aircrafts. Sizing codes for turbojet, turboshaft, and hybrid engines are also available for auto-building engine models for transient analysis. Libraries are available for air cycle and vapor cycle refrigeration systems, and electrical subsystem components.

D. Conventional Propulsive and TMS System

Propulsive power for the air vehicle platform was conventionally provided by a notional turboprop engine, with design characteristics similar to those found in [19]. Flight power requirements for the mission were ensured by designing the engine at sea level static, ISA conditions. The turbine engine will also serve as the prime mover for the subsequent series-hybrid architecture, whose impact on vehicle level performance was investigated.

The turbomachinery for the proposed prime mover consists of a two-stage centrifugal compressor and three-stage axial turbine [19]. ATTMOSphere turbomachinery graphical user interfaces, provide a means to size the desired turbomachinery, and generate performance maps to accommodate off-design performance. The turboshaft is connected to a propeller via a gear box with shafts operating at design speeds of 2000 rpm for the propeller and 41700 rpm for the turboshaft. Fuel to air ratio (FAR) at the combustor was calculated based on the reference air flow rates and TSFC, while the nozzle exit area was calculated based on an assumed exit Mach number, and design turboshaft power.

Fig. 3 illustrates the baseline turboprop engine model. Bleed flows and shaft power extractions are shown as connections in the engine, but were not used for this study. In support of off-design operation, two sets of controls were incorporated. The primary control varies the FAR of the combustor in order to match the aircraft's required thrust. A secondary control was added in which the blade angle of the propeller is varied to operate the turboshaft at an optimal speed. The pressure ratio associated with a maximum efficiency for a given shaft speed is known from the compressor performance maps. By varying the propeller blade angle, the turboshaft speed can be adjusted up or down to operate the compressors at a more efficient operating point. It was found that turbine efficiency did not vary enough to be incorporated into this control strategy but use of this control consistently reduced the overall fuel burn of engines throughout this study.

For the conventional propulsive subsystem, waste heat generation sources were grouped under aircraft "auxiliary" loads (radar, flight control actuation, housekeeping). Correspondingly, a ram air based thermal management system, as seen in Fig. 3, was designed to accommodate 8 kW of heat dissipation. The transient variation in auxiliary heat load may be seen in Fig. 4. The auxiliary heat load experiences step changes during the endpoints of the loiter interval to emulate the switch between standby and active operational modes of the radar, and vice versa. Detailed modeling of the heat acquisition system for the auxiliary heat loads is foregone in place of a simpler characterization represented by a PAO loop which rejects its heat through a ram air/oil heat exchanger. Assumed requirements on radar system operation require PAO temperatures to be less than 55 F. A valve regulates the amount of ram air to satisfy the PAO exit temperature requirement, while the flow itself exhausted to ambient.

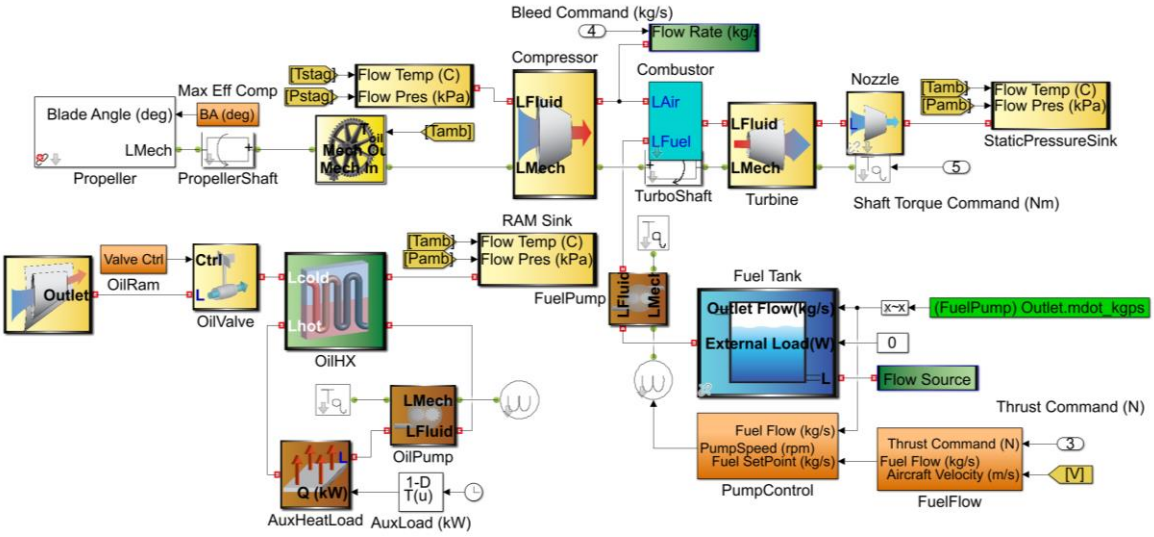

Fig. 3 Baseline turboprop engine and thermal management system

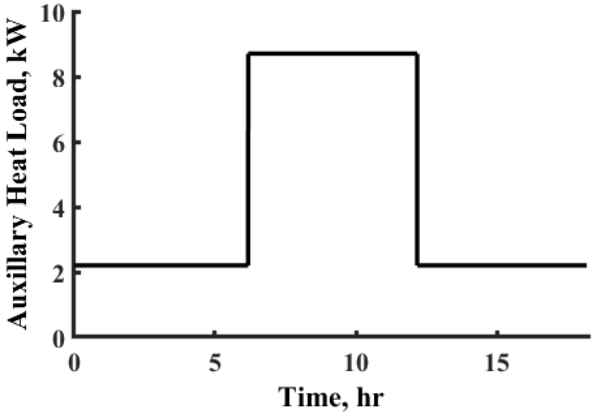

Fig. 4 Auxiliary heat load variation

2. Mission Analysis Results

The developed propulsive and thermal management system models were integrated with the 2.5DoF air vehicle model to perform an integrated system simulation of the mission in Fig. 2. The engine weight at the beginning of the mission consists of 4901 lb of empty weight, of which approximately 372 lbs results from the turboshaft components, and 7000 lb of fuel for a total of 11901 lb. Figure 5 provides the resulting thrust required from the engine. In the integrated engine study, the baseline engine burned approximately 4240 lb of fuel which served as a critical benchmark when developing the series-hybrid engine. An additional critical engine metric of engine FAR is provided in Fig. 6a. The engine operates at a high FAR (greater than 0.03) early in the mission, which could potentially lead to an overheat condition at the turbine inlet, as shown in Fig. 6b. Fig. 7a provides the turboshaft speed throughout the mission, and Fig. 7b shows the variation in propeller blade angle which drives the turboshaft to an optimal speed per the control described earlier in the report. Figure 8a illustrates the ram air flow requirements required to reject the heat generated by the auxiliary heat loads. It is seen that approximately 0.5 lbm/s of air are required during the loiter segment when the radar is in active operation mode, while peak flow rates greater than 1 lbm/s are required during initial climb and the end of descent. In Fig. 8b, PAO temperatures exiting the radar are seen to remain below the 55 F limit.

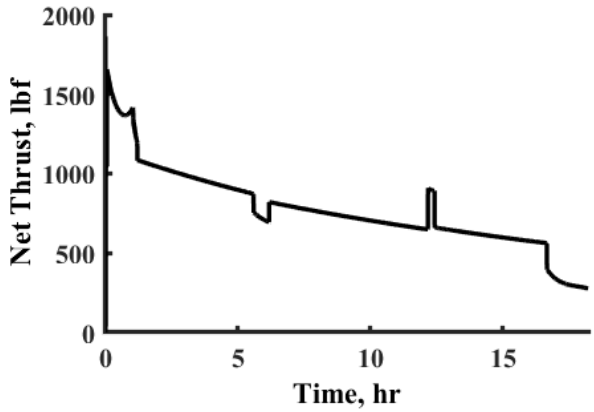

Fig. 5 Integrated engine thrust

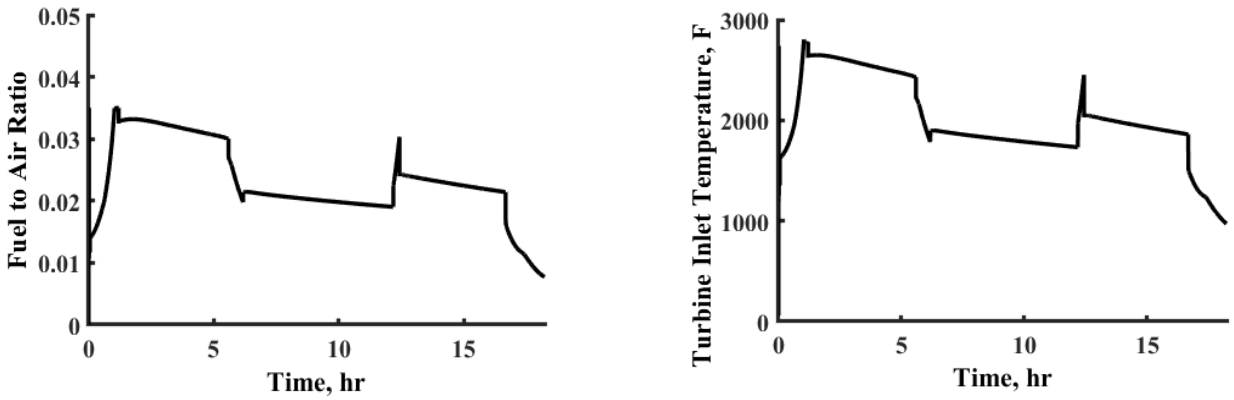

a) b)

Fig. 6 Integrated engine fuel – air ratio and turbine inlet temperature

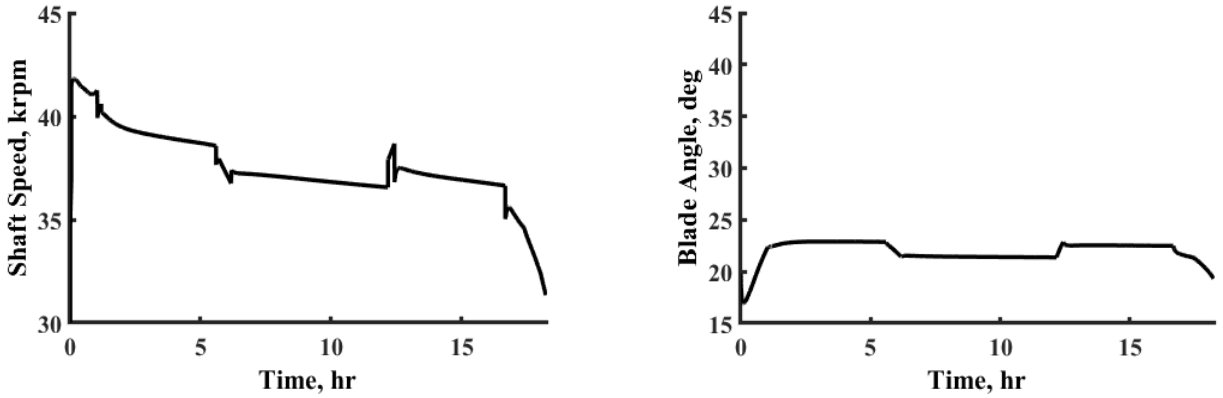

a) b)

Fig. 7 Optimal turboshaft speed and propeller blade angle

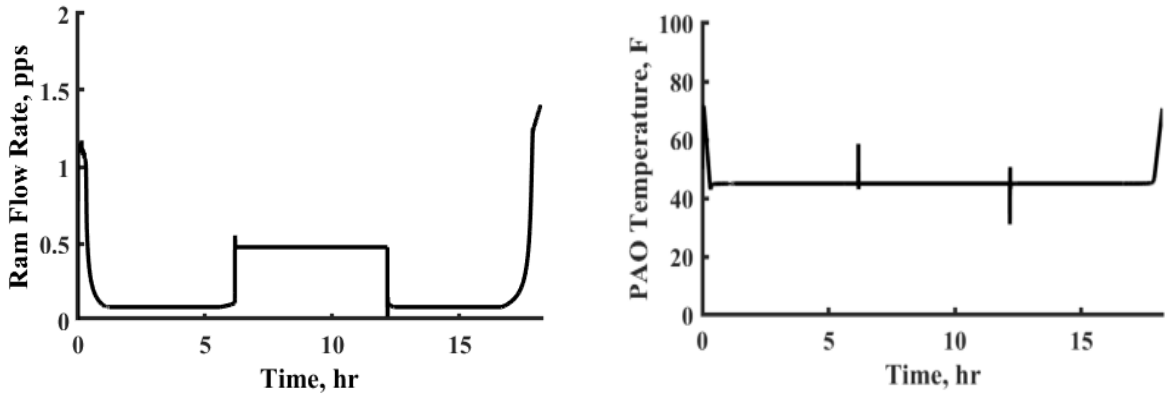

a) **b)**

Fig. 8 Conventional turboprop engine ram air flow rate and maximum PAO temperature

E. Series-Hybrid Propulsive and TMS System Design and Analysis

1. Initial Explorative Study of Propulsion System Performance

The conventional turboprop engine which served as a baseline propulsion system was incorporated within a series hybrid-electric architecture, as seen in Fig. 9. As an initial design study, battery usage was employed during climb and the initial cruise segment to offset flight power requirements during those mission phases. Estimates for the required battery power and weight were determined by known flight power requirements from the baseline mission and assumed losses for the generator and motor. For this initial explorative study, turboshaft output power was limited to 400 kW, with the battery supplying 200 kW during the climb segment, and 100 kW during the initial cruise segment, after which battery usage would cease for the remainder of the mission. By analyzing the individual performance of the turboshaft and electric drive train throughout the mission, updates could be made as to the flight condition where the turboshaft could be more efficiently designed, and choose better battery utilization strategies.

The design process for the battery and electrified drive train components required several assumptions regarding battery energy density and generator and motor losses. The PMSM generator was sized at a reduced shaft speed of 20000 rpm and an 800 kW design, while the PMSM motor was sized at a shaft speed of 15000 rpm and 900 kW design to account for losses associated with the generator and motor. The electrical components were sized to 1000 V. The turboshaft and propeller components were kept the same with a large, idealized lithium-polymer battery of 1045 lb added to the architecture. The battery was assumed to operate at 115 W-hr/lb with 455 W/lb. Given the increased complexity of the series-hybrid engine, several controls were utilized. The primary control in the new architecture is the motor torque which is commanded via a built-in rectifier to provide the command thrust required from the engine. One benefit of the series-hybrid engine is that the propeller shaft and turboshaft are now decoupled, so optimal shaft speed controls were added for multiple shafts where propeller blade angle is controlled to operate the propeller shaft at a maximum efficiency while the FAR of the combustor is now controlled to operate the turboshaft at an optimal shaft speed. The final control utilizes the built-in rectifier for the generator torque to operate the battery at a power dictated by a pre-determined schedule. For this study with known altitude, Mach, and anticipated turboshaft powers, a pre-fixed schedule was deemed acceptable but a more sophisticated control responsive to dynamics resulting from changes in missions and engine performance would be more desirable. The turboshaft fuel burn was found to be comparable to the baseline engine (4190 lb of fuel burn), but the added weight associated with the series-hybrid components makes this an undesirable design. However, the study highlighted a critical performance change in a series-hybrid configuration relative to the standalone baseline engine that could be manipulated for sizing a new turboshaft. The addition of a battery reduces the maximum turboshaft power requirements during the takeoff and climbing segments of the mission, as highlighted in Fig. 10a. This allows for sizing of a new turboshaft to a reduced power and a reduced TSFC relative to the standalone baseline engine. The engine operates near a TSFC of 0.3 lb/lbf-hr for a significant portion of the mission as shown in Fig. 10b, but a value closer to 0.2 lb/lbf-hr could be achievable for a higher PR turboshaft design. Assembling a new series-hybrid architecture with reduced battery weight and a more efficient turboshaft engine could allow for an overall weight reduction in a series-hybrid design.

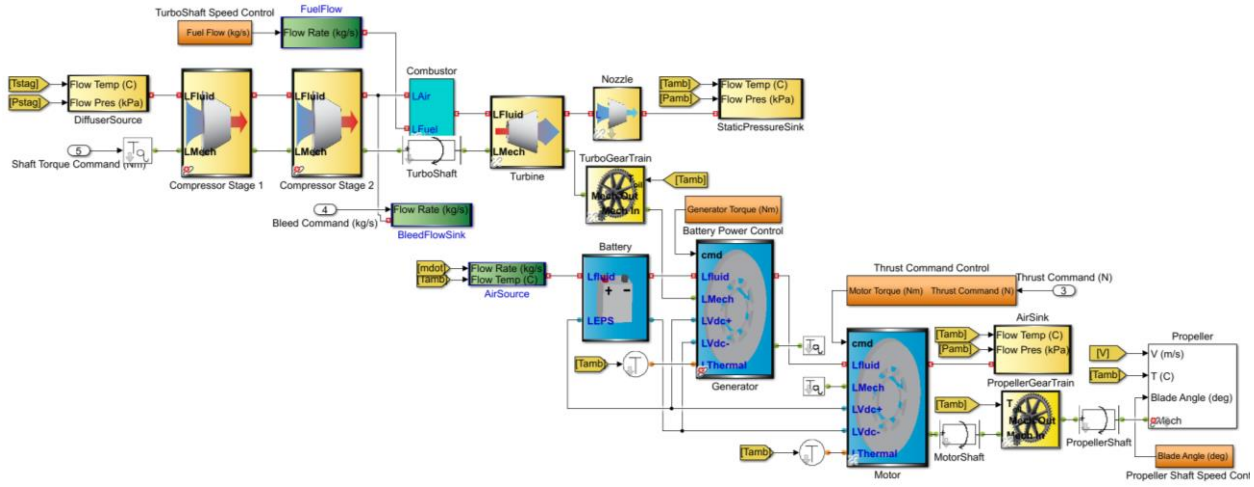

Fig. 9 Series-hybrid propulsive architecture

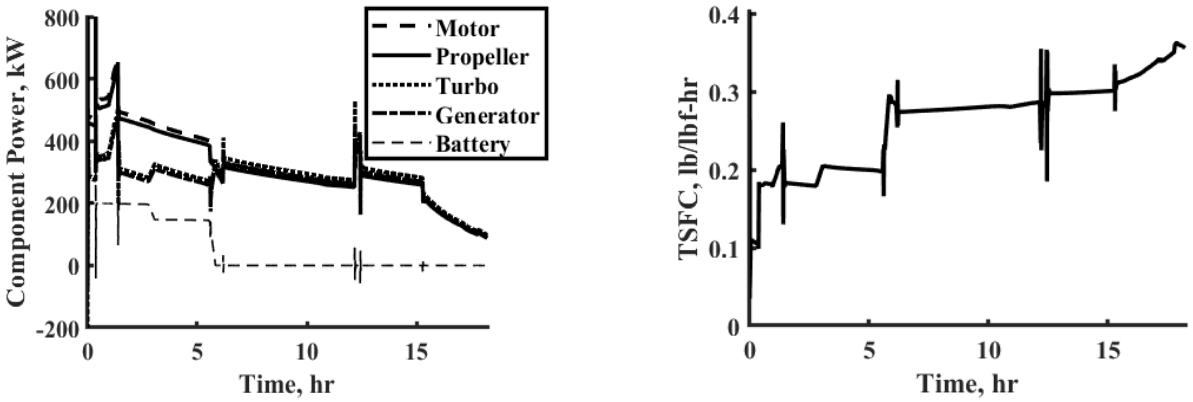

a) **b)**

Fig. 10 Critical series-hybrid component powers and thrust specific fuel consumption

2. Redesign of Series-Hybrid Propulsive Subsystem

Analysis of the initial hybrid architecture with its associated battery utilization method revealed fuel burn comparable to the baseline engine, in addition to a heavy battery required to maintain a state of charge between 0.2 – 0.3. An updated battery utilization schedule was selected, limiting operation to climb only. The turboshaft was re-designed to provide 600 kW of power, with a desired TSFC of 0.225 lb/lbf-hr. A design altitude of 26000 ft, Mach = 0.275, and maximum turbine inlet temperature of 2300 F. Generic propeller performance maps were incorporated into these engine designs [20], and a slight increase in propeller diameter to 2.9 m was incorporated into the new engine sizing routine, still with a design speed of 2000 rpm. The turboshaft engine sizing calculations are detailed in the equations below. TSFC is fixed with FAR varied in order to balance turbine, compressor, and propeller powers. A nozzle exit Mach number of 0.3 was chosen and compressor and turbine efficiencies of 82% and 89% were assumed respectively.

$$\dot{m}_f = (\mathrm{TSFC})\mathbf{T_{net}} \tag{1}$$

$$\dot{m}_c = \dot{m}_f\left(\frac{1}{\mathrm{FAR}}\right) \tag{2}$$

$$T_{tc} = T_{max} - \eta_c Q_c \frac{\mathrm{FAR}}{c_p} \tag{3}$$

$$P_{tc} = \left[\eta_{comp}\left(\frac{T_{tc}}{T_{tair}} - 1\right) - 1\right]^{\gamma/\gamma-1} P_{tair} \tag{4}$$

$$PR_{comp} = \frac{P_{tc}}{P_{tair}} \tag{5}$$

$$\dot{m}_{comp} = \dot{m}_c \tag{6}$$

$$Q_{comp} = \dot{m}_{comp}\frac{c_p T_{tair}}{\eta_{comp}}\left(PR_{comp}^{\gamma-1/\gamma} - 1\right) \tag{7}$$

$$\dot{m}_t = \dot{m}_c + \dot{m}_f \eta_c \tag{8}$$

$$P_{tn} = \left(1 + \frac{\gamma - 1}{2} M_n^2\right)^{\gamma/\gamma-1} P_s \tag{9}$$

$$\mathbf{T_{noz}} = \dot{m}_n \sqrt{\left[1 - \left(\frac{P_s}{P_{tn}}\right)^{\gamma-1/\gamma}\right] 2 c_{pn} T_{tn}} \tag{10}$$

$$\mathbf{T_{net}} = \mathbf{T_{prop}} + \mathbf{T_{noz}} - \dot{m}_c v_{AC} \tag{11}$$

$$\mathrm{PR}_t = \frac{P_{tc}}{P_{tn}} \tag{12}$$

$$Q_t = \dot{m}_t c_p T_t \eta_{turb}\left[1 - \left(\frac{1}{PR_{turb}}\right)^{\gamma-1/\gamma}\right] \tag{13}$$

$$T_{tn} = T_{max}\left(1 - \eta_t\left[1 - \left(\frac{1}{PR_{turb}}\right)^{\gamma-1/\gamma}\right]\right) \tag{14}$$

where M_n is the nozzle exit Mach number, $\mathbf{T}$ is thrust, $\dot{m}_f$ is fuel flow rate, $\dot{m}_c$ is combustor inlet air flow rate, c_p is air specific heat, Q_c is the heat of combustion of fuel, η_c is the combustor efficiency, T_{max} is the maximum turbine inlet temperature, T_{tc} is the combustor inlet temperature, P_{tc} is the combustor inlet pressure, T_t is the engine inlet temperature, P_t is the engine inlet pressure, γ is the specific heat ratio of air, η_{comb} is the compressor efficiency, $\dot{m}_{comp}$ is the compressor inlet air flow rate, Q_{comp} is the compressor power, $\dot{m}_t$ is the turbine inlet air/fuel mixture flow rate, P_{tn} is the nozzle inlet total pressure, P_s is the ambient pressure, $\dot{m}_n$ is the nozzle flow rate, c_{pn} is the nozzle air specific heat, T_{tn} is the nozzle inlet total temperature, v_{AC} is the aircraft velocity, and Q_t is the turbine work. With the previously defined boundary conditions and performance requirements of the new turboshaft, the resulting turboshaft architecture operates at an air flow of approximately 3.1 lb/s with an overall compressor PR of 25, as compared to the baseline turboshaft which operates at an approximate air flow of 7.5 lb/s and overall compressor PR of 11. The design operates at a reduced flow rate, and significantly increased PR relative to the baseline engine but also at a reduced FAR of 0.024 ensuring that turbine inlet temperature does not become too high during high thrust requirements.

As the turboshaft power requirements were reduced, the PMSM generator was also resized to a reduced power of 600 kW. A 550 lb battery was added in the updated architecture. Similar controls to the initial hybrid architecture design for propeller shaft speed, turboshaft speed, and engine thrust were incorporated into the new series-hybrid architecture. However, generator voltage is now commanded according to a pre-fixed turboshaft power instead of a pre-fixed battery power. This control was found to be more a more numerically robust approach in this configuration. As previously mentioned, a more sophisticated control capable of adjusting to changes in ambient, boundary conditions, and engine performance would ideally be implemented in future studies.

3. Thermal Management System

Waste heat generation sources upon the series-hybrid aircraft were consolidated into two groups: electrical devices from the drive train, and aircraft auxiliary loads. A thermal management system, as seen in Fig. 11, was designed to accommodate loads of 30 kW and 8 kW of heat dissipation from the drive train, and auxiliary heat loads, respectively. The existing auxiliary heat load variation from the baseline case is augmented by the transient heat load profile associated with electrical devices in the drive train, as seen in Fig. 12.

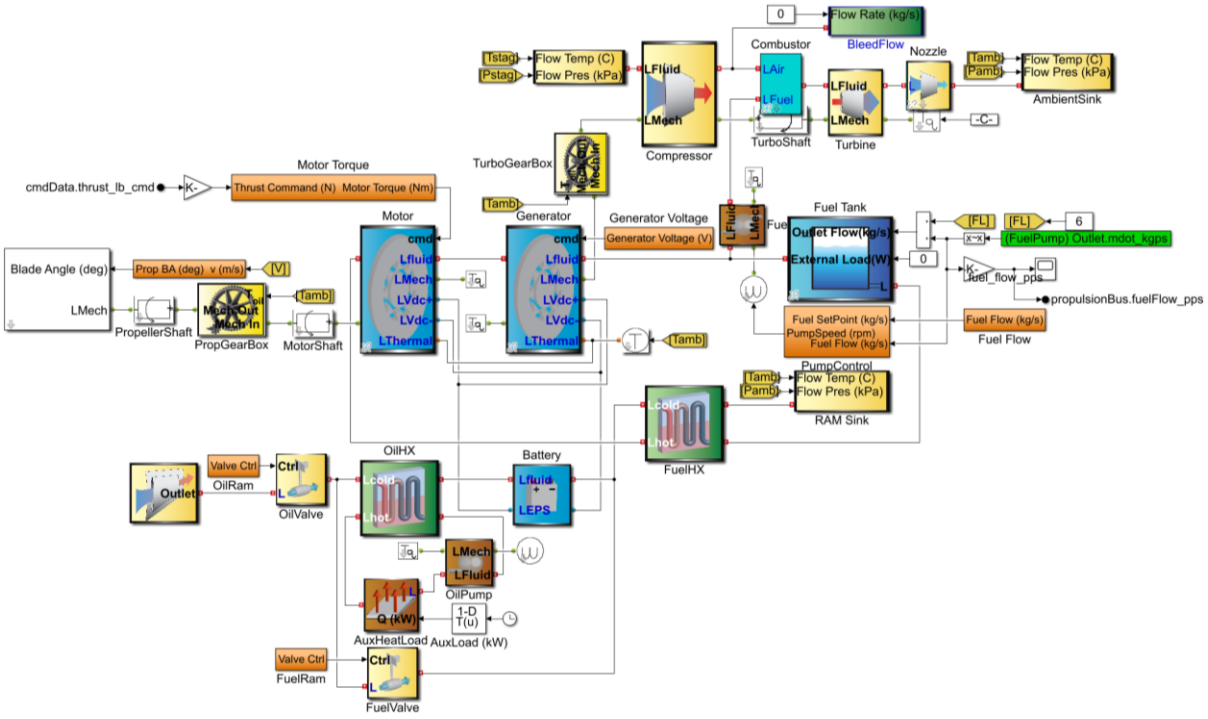

Fig. 11 Integrated series-hybrid architecture with thermal management system

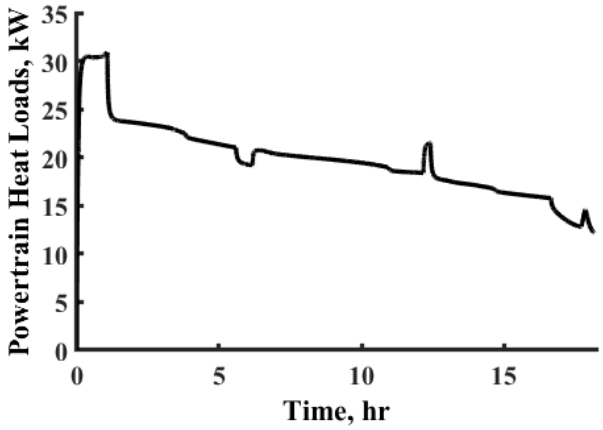

Fig. 12 Powertrain heat loads

The proposed TMS interacts with the hybrid propulsion system through a split in the fuel supply line which feeds the turboshaft combustor. This design decision was driven by the relatively high temperature operation (<= 350 F) of the motor and generator. Fuel was pumped at a fixed flow rate of 13.2 lb/s, which was found to be the flow rate required to ensure that internal temperatures of the generator and motor stay below 350 F.

Given the high fuel temperatures expected within the TMS fuel loop, ram air was chosen for cooling auxiliary heat loads. As in the baseline case, detailed modeling of the heat acquisition system for the auxiliary heat loads is foregone in place of a simpler characterization represented by a PAO loop which rejects its heat through a ram air/oil heat exchanger. Battery temperatures are controlled to be maintained beneath a 105 F threshold to avoid capacity fade and premature degradation [21]. Previous design iterations of the TMS indicated that this requirement was not met while using fuel as a thermal sink. Therefore, ram air was chosen to provide the required cooling for the battery. Two sets of valves downstream of the ram air inlet control air flow to ensure that the maximum PAO loop temperature stays below 55 F, while the temperature of the recirculated fuel at the tank inlet is less than 160 F. The primary ram valve is controlled to maintain the PAO loop maximum temperature. Ram air enters the PAO/air HX, passes through the battery, and finally cools fuel through the fuel/air HX prior to being dumped to ambient. A secondary valve ahead of the PAO/air HX pulls additional ram air directly to the fuel/air HX to ensure that the maximum fuel temperature is not exceeded. The set of valves implemented in this manner ensures that the minimum amount of ram air is pulled into the engine, thus minimizing the impact on vehicle drag. No active controls were required for the battery, as the battery did not approach temperature limits. While the PAO/air HX was sized to an 8 kW design, a 15 kW fuel/air HX design was required to provide sufficient ram air cooling of the fuel loop. The auxiliary heat load during cruise requires more ram air than the fuel, and as such, ram flow rate during cruise is approximately the same between the baseline and hybrid architectures. During climbing and descent segments, however, the fuel requires more ram air than is being drawn to cool the auxiliary heat loads, and is therefore draws more ram than the conventional turboprop during those portions of the mission.

4. Mission Analysis Results

The total weight of the series-hybrid engine at the start of the mission was set to be the same as the baseline engine. As the weight of the series hybrid turboshaft, motor, generator, battery, and supporting TMS was calculated as 1080 lb as compared to the 372 lb baseline engine, the empty weight of the series-hybrid engine was increased to 5609 lb while the fuel weight was reduced to 6292 lb. With the new series-hybrid turboshaft and TMS architectures designed and integrated with the 2.5 DoF model, the resulting fuel burn of the new series-hybrid engine under the same altitude and Mach schedule was calculated as 3450 lb; a reduction in fuel burn of 750 lb relative to the standalone baseline engine study. This result suggests that the added empty weight of 708 lb in the series-hybrid engine is offset by 750 lb in reduced fuel burn. In this study though, as the aircrafts start their missions at the same total weight, the baseline engine is reducing its total aircraft weight faster than the series-hybrid, which does provide some power and thrust benefits relative to the series-hybrid engine. Figure 13a provides critical component powers for the new engine and net thrust. Figure 14 provides the state of charge of the battery and engine TSFC. While battery power is relatively low throughout the bulk of the mission, with most of its use occurring during the climbing portion of the mission,

without its additional power in the early portion of the mission the turboshaft would not be able to provide enough thrust to achieve the mission requirements for the engine. The engine TSFC operates near the design of 0.225 lb/lbf-hr throughout the bulk of the mission while slowly climbing later in the mission when engine power and thrust requirements begin to decline. The FAR of the new engine is provided in Fig. 15a, and is significantly reduced relative to the baseline engine, resulting in a decreased turbine inlet temperature despite the increased PR of the engine, as highlighted in Fig. 15b. Additional engine mechanical heat losses associated with ball bearings, friction, shaft operation, etc. are not accounted for in this study, but could be significant in the engines. Given the reduced power of the turboshaft in the hybrid engine, relative to the baseline design, some of these losses may be reduced in the series-hybrid engine, but a more detailed analysis of this type of heat transfer and additional TMS should be performed in the future, including the addition of oil cooling of turbomachinery and other mechanical components.

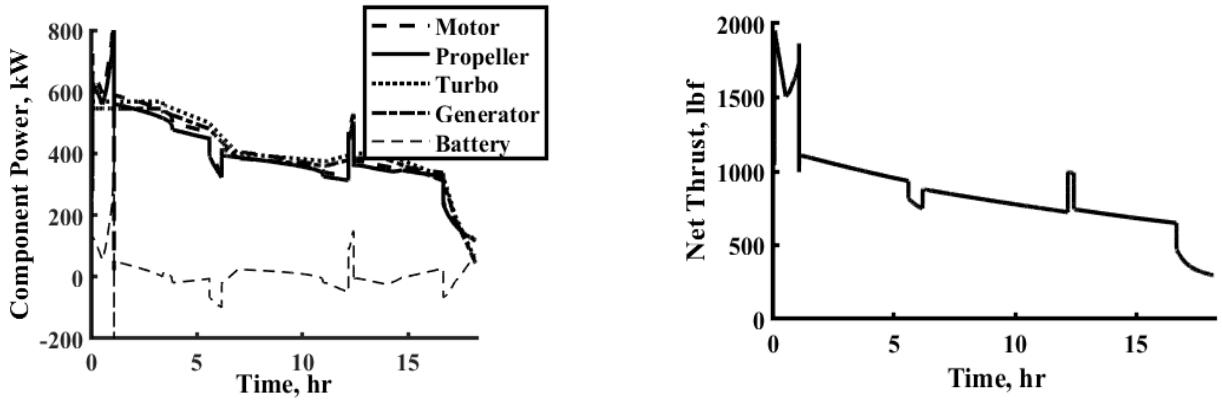

a) **b)**

Fig. 13 Critical integrated series-hybrid architecture component powers and net thrust

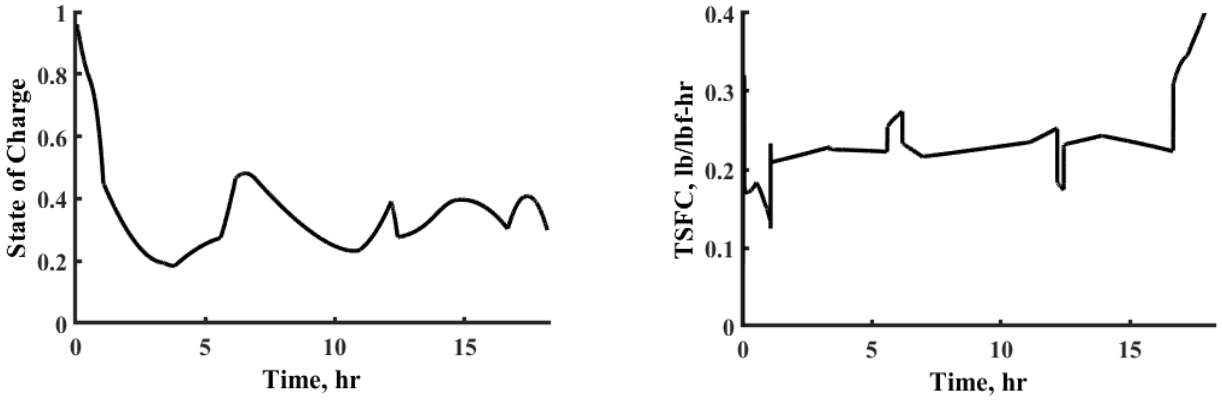

a) **b)**

Fig. 14 State of battery charge and thrust specific fuel consumption in integrated series-hybrid architecture

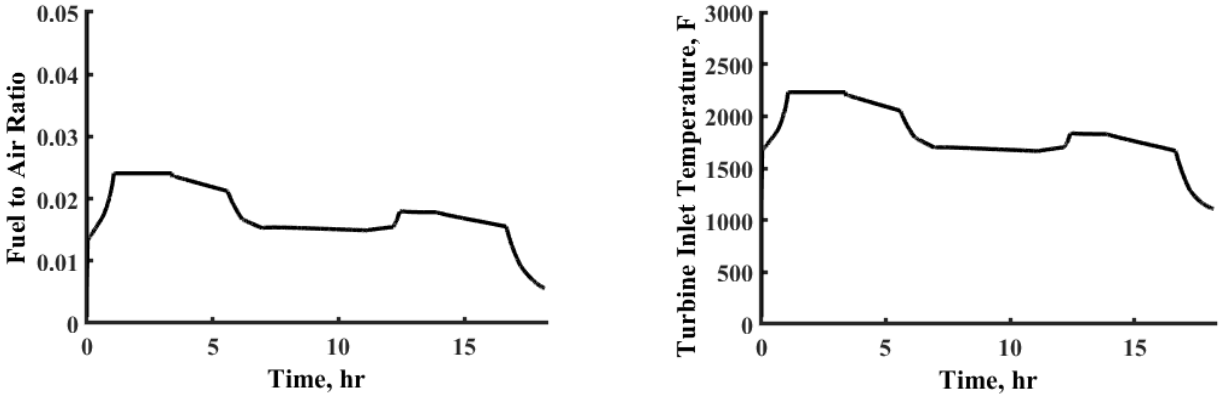

a) **b)**

Fig. 15 Fuel-air ratio and turbine inlet temperature of integrated series-hybrid architecture

The turboshaft speed and propeller shaft speed controls are highlighted in Fig. 16 and Fig. 17a, which provide turboshaft and propeller shaft speeds resulting from the commanded FAR and propeller blade angle, also provided in Fig. 17b. Voltages and current from the generator, motor, and battery are plotted in Fig. 18. Given the idealized battery component utilized in this study, little change in DC voltage occurs across the electrical components throughout the mission despite the large change in state of charge of the battery. The resulting ram air flow rate is provided in Fig. 20, along with the fuel tank inlet temperature and radar outlet temperature in the PAO loop highlighting that maximum temperatures for the fuel and PAO are not exceeded.

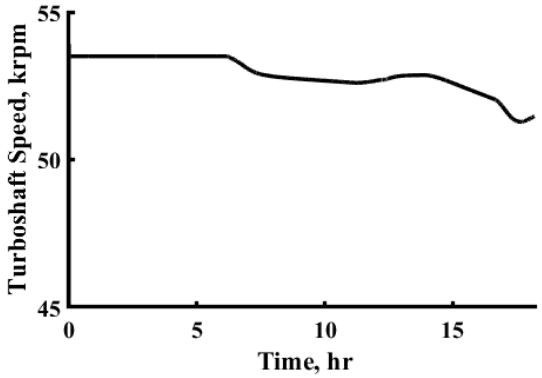

Fig. 16 Optimal turboshaft speed of integrated series-hybrid architecture

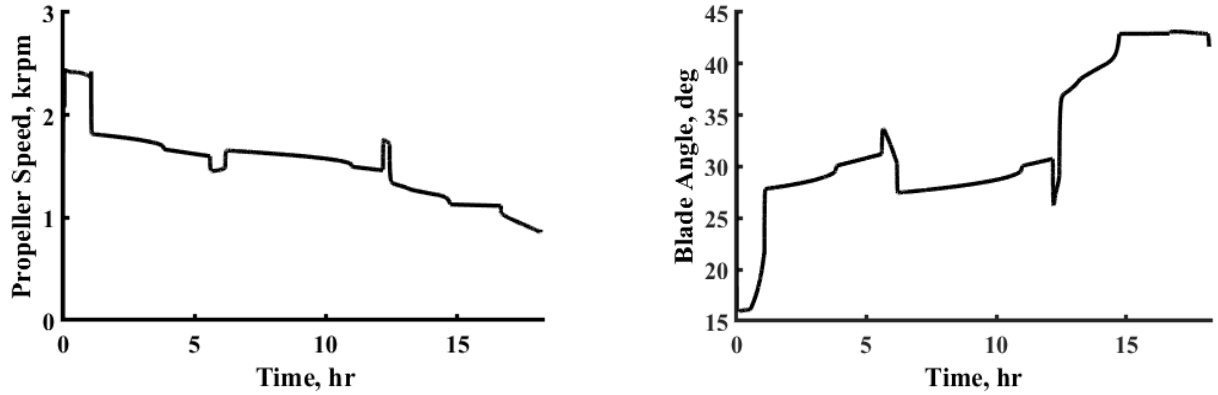

a) b)

Fig. 17 Optimal propeller shaft speed and blade angle of integrated series-hybrid architecture

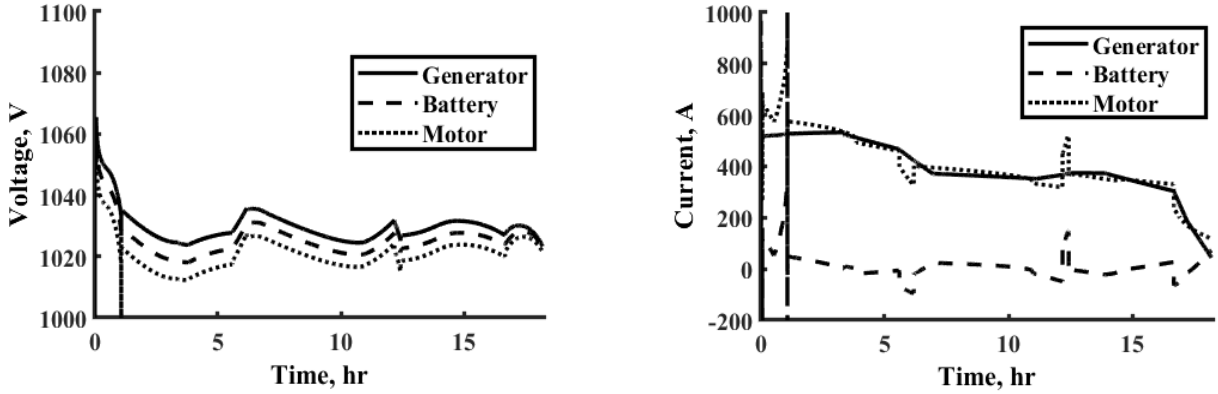

a) b)

Fig. 18 DC voltage and current of integrated series-hybrid architecture

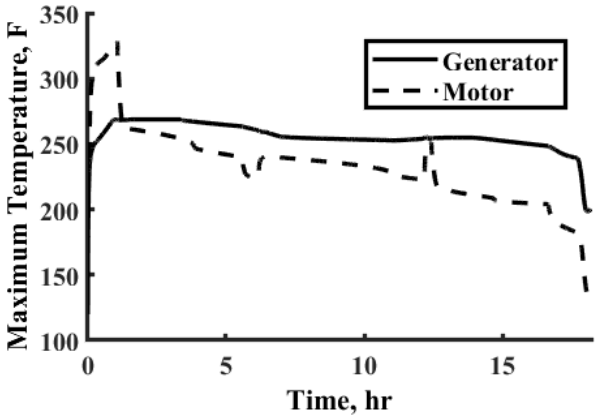

Fig. 19 Generator and motor maximum internal temperatures in integrated series-hybrid architecture

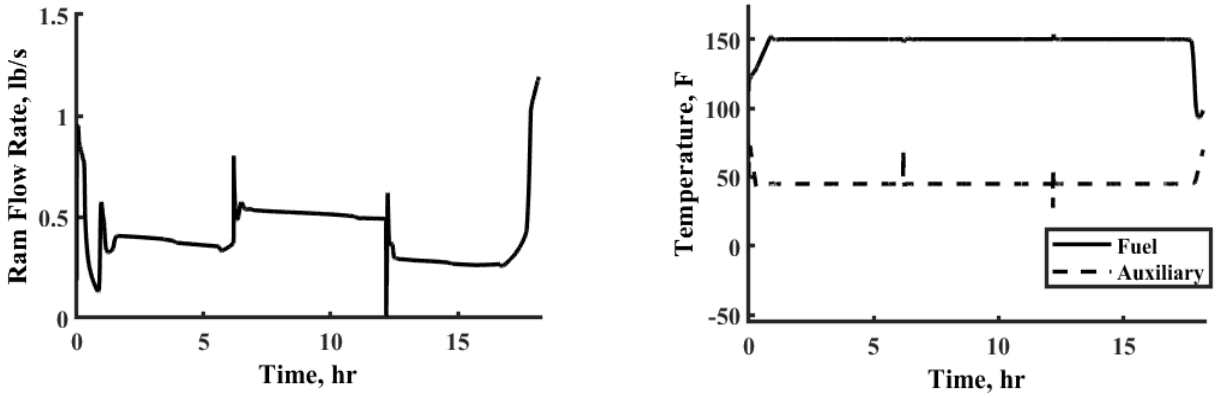

a) **b)**

Fig. 20 TMS ram-air flow rate, along with fuel tank inlet and radar outlet temperatures in integrated series-hybrid architecture

V. Conclusions

Studies in the literature indicated that significant thermal management requirements associated with adopting hybrid electric architectures for aircraft may offset their anticipated performance benefits. This paper addresses this concern by using integrated simulations of propulsive, thermal, and flight dynamics models to account for interactions between these subsystems, and obtain optimal vehicle performance for a candidate 11901 lb. vehicle which will fly a notional 18 hour mission. In particular, the current study investigated the potential fuel savings offered by utilizing a series hybrid architecture, whose prime mover was chosen to be a turboshaft engine, with similar design performance to that found in [19]. As an initial estimate of hybrid electric engine performance, the battery was utilized during the climb and initial cruise phases of the mission. Fuel burn was found to be comparable to the baseline propulsion system, and a heavy battery was required to ensure that the minimum battery state of charge remained between 0.2 – 0.3. As an attempt to obtain improved fuel burn and decreased battery weight, battery utilization was limited to climb only, and the prime mover was redesigned for more efficient performance at an altitude of 26000 ft, and M = 0.275 operating condition, which substantially reduced fuel burn with respect to the conventional propulsion system. A thermal management system was proposed to reject the heat generated from electrical components within the hybrid drive train, as well as auxiliary loads onboard the aircraft, which were comprised of a radar, actuation, and

housekeeping loads. The TMS was integral with the propulsion system through a fuel loop whose source was the main fuel tank for the prime mover combustor. A closed fuel loop was utilized to cool the motor and generator given their relatively high operating temperatures, while an intermediate PAO loop was used to cool the aggregate auxiliary heat loads. An open ram air circuit was used as the heat sink for the auxiliary loads, as well as the TMS fuel loop prior to re-entering the fuel tank. Maximum temperatures for the motor, generator, battery, and fuel were maintained under the proposed TMS architecture. With respect to the baseline propulsion system, a fuel savings of 750 lb. was obtained despite a gain of 708 lb. associated with the added weight of electrical devices within the drive train. Future studies will focus on incorporating further detail regarding the heat loads associated onboard the aircraft for increased fidelity in predicting vehicle performance when utilizing hybrid electric architectures.

References

[1] Wall, T.J., Meyer, R.T., "A Survey of Hybrid Electric Propulsion for Aircraft," AIAA Paper 2017-4700, July 2017 doi: 10.2514/6.2017-4700

[2] Bradley, M.K., Droney, C.K., "Subsonic Ultra Green Aircraft Research: Phase II – Volume II – Hybrid Electric Design Exploration", NASA/CR-2015-218704/ Volume II

[3] Hiserote, R. M., "Analysis of Hybrid Electric Propulsion Designs for Small Unmanned Aircraft Systems," M.S. Thesis, Aeronautics and Astronautics Dept., Air Force Institute of Technology, Wright Patterson Air Force Base, OH, 2010.

[4] Cinar, G., "A Methodology for Dynamic Sizing of Electric Power Generation and Distribution Architectures," Ph.D. Dissertation, School of Aerospace Engineering, Georgia Tech, Atlanta, GA, 2018

[5] Finger, D.F., Braun, C., Bil, C., "An Initial Sizing Methodology for Hybrid-Electric Light Aircraft," AIAA Paper 2018-4229, June 2018, doi: 10.2514/6.2018-4229

[6] de Vries, R., Brown, M., Vos, R., "A Preliminary Sizing Method for Hybrid-Electric Aircraft Including Aero-Propulsive Interaction Effects," AIAA Paper 2018-4228, June 2018, doi: 10.2514/6.2018-4228

[7] Aigner, B., Stumpf, E., Hinz, A., De Doncker, R.W., "An Integrated Design Framework for Aircraft with Hybrid Electric Propulsion," AIAA Paper 2018-4228, June 2018, doi: 10.2514/6.2018-4228

[8] McCluskey, F. P., Saadon, Y., Yao, Z., Shah, J., "Thermal Management Challenges in Turbo-Electric and Hybrid Electric Propulsion," AIAA Paper 2018-4695, July 2018, doi: 10.2514/6.2018-4695

[9] Rheaume, J., Lents, C.J., "Design and Simulation of a Commercial Hybrid Electric Aircraft Thermal Management System," AIAA Paper 2018-4994, July 2018, doi: 10.2514/6.2018-4994

[10] Kim., J.H., Kwon, K.S., Roy, S., Garcia, E., Mavris, D., "Megawatt-class Turboelectric Distributed Propulsion, Power, and Thermal Systems for Aircraft," AIAA Paper 2018-2024, Jan. 2018, doi: 10.2514/6.2017-2024

[11] Walters, E. A., Iden, S., McCarthy, K., Amrhein, M., O'Connell, T., Raczkowski, B., Wells, J., Lamm, P., Wolff, M., Yerkes, K., Borger, W., Wampler, B., "INVENT Modeling, Simulation, Analysis, and Optimization", AIAA 2010-287, January 2010

[12] McCarthy, P., McCarthy, K., Hasan, M., Boyd, M., "A Multi-Domain Component Based Modeling Toolset for Dynamic Integrated Power and Thermal System Modeling" SAE Technical Paper 2019-01-1385, 2019, doi: 10.4271/2019-01-1385

[13] Shimmin, K., Russell, G., Reuter, R., Iden, S., "Development and Performance of a Reduced Order Dynamic Aircraft Model" SAE Technical Paper 2015-01-2415, 2015, doi: 10.4271/2015-01-2415

[14] McCarthy, K., Walters, E., Heltzel, A., Elangovan, R. et al., "Dynamic Thermal Management System Modeling of a More Electric Aircraft," SAE Technical Paper 2008-01-2886, 2008, doi: 10.4271/2008-01-2886

[15] McCarthy, P., Niedbalski, N., McCarthy, K., Walters, E. et al., "A First Principles Based Approach for Dynamic Modeling of Turbomachinery," SAE Technical Paper 2016-01-1995, 2016, doi: 10.4271/2016-01-1995

[16] Kania, M., Koeln, J., Alleyne, A., McCarthy, K., et al., "A Dynamic Modeling Toolbox for Air Vehicle Vapor Cycle Systems," SAE Technical Paper 2012-01-2172, 2012, doi: 10.4271/2012-01-2172

[17] McCarthy, K., McCarthy, P., Wu, N., Alleyne, A., et al., "Model Accuracy of Variable Fidelity Vapor Cycle: System Simulations," SAE Technical Paper 2014-01-2140, 2014, doi: 10.4271/2014-01-2140

[18] https://aerospace.honeywell.com/en

[19] Frignac, J. P. and Privoznik, E. J., "The Growth and Evolution of the TPE331", Gas Turbine Conference & Exhibit & Solar Energy Converence, San Diego, CA, March, 1979

[20] Unified Propulsion Lecture #1, MIT, 2018

[21] MacDonald, M., Rheaume, J., Khakpour, Y., Lents, C., "Transient Cooling Approach for a Mhr Class Hybrid Electric Propulsion System Battery Pack", AIAA Paper 2020-0120, Jan 2020, doi: 10.2514/6.2020-0120